the plant journal

SEB SOCIETY FOR EXPERIMENTAL BIOLOGY

The Plant Journal (2009) **60**, 303–313 doi: 10.1111/j.1365-313X.2009.03955.x

Lipid microdomain polarization is required for NADPH oxidase-dependent ROS signaling in *Picea meyeri* pollen tube tip growth

Peng Liu[1,2,†], Rui-Li Li[1,2,†], Liang Zhang[1,2], Qin-Li Wang[1], Karsten Niehaus[3], František Baluška[4], Jozef Šamaj[4,5,6] and Jin-Xing Lin[1,*]

[1]*Key Laboratory of Photosynthesis and Molecular Environmental Physiology, Institute of Botany, Chinese Academy of Sciences, Beijing 100093, China,*

[2]*Graduate School of the Chinese Academy of Sciences, Beijing 100049, China,*

[3]*Faculty of Biology, Department of Proteome and Metabolome Research, Bielefeld University, D-33594 Bielefeld, Germany,*

[4]*Institute of Cellular and Molecular Botany, Rheinische Friedrich-Wilhelms-University Bonn, Department of Plant Cell Biology, Kirschallee 1, D-53115 Bonn, Germany,*

[5]*Institute of Plant Genetics and Biotechnology, Slovak Academy of Sciences, Akademicka 2, SK-95007 Nitra, Slovak Republic, and*

[6]*Faculty of Science, Palacký University, 78371 Olomouc, Czech Republic*

Received 7 May 2009; revised 8 Jun 2009; accepted 9 Jun 2009; published online 23 July 2009.
*For correspondence (fax +86 10 62836211; e-mail linjx@ibcas.ac.cn).
†These authors contributed equally to this work.

SUMMARY

The polarization of sterol-enriched lipid microdomains has been linked to morphogenesis and cell movement in diverse cell types. Recent biochemical evidence has confirmed the presence of lipid microdomains in plant cells; however, direct evidence for a functional link between these microdomains and plant cell growth is still lacking. Here, we reported the involvement of lipid microdomains in NADPH oxidase (NOX)-dependent reactive oxygen species (ROS) signaling in *Picea meyeri* pollen tube growth. Staining with di-4-ANEPPDHQ or filipin revealed that sterol-enriched microdomains were polarized to the growing tip of the pollen tube. Sterol sequestration with filipin disrupted membrane microdomain polarization, depressed tip-based ROS formation, dissipated tip-focused cytosolic Ca^{2+} gradient and thereby arrested tip growth. NOX clustered at the growing tip, and corresponded with the ordered membrane domains. Immunoblot analysis and native gel assays demonstrated that NOX was partially associated with detergent-resistant membranes and, furthermore, that NOX in a sterol-dependent fashion depends on membrane microdomains for its enzymatic activity. In addition, *in vivo* time-lapse imaging revealed the coexistence of a steep tip-high apical ROS gradient and subapical ROS production, highlighting the reported signaling role for ROS in polar cell growth. Our results suggest that the polarization of lipid microdomains to the apical plasma membrane, and the inclusion of NOX into these domains, contribute, at least in part, to the ability to grow in a highly polarized manner to form pollen tubes.

Keywords: di-4-ANEPPDHQ, lipid microdomains, NADPH oxidase, pollen tube, reactive oxygen species.

INTRODUCTION

The cytoplasmic membrane contains sterol/sphingolipid-enriched liquid-ordered lipid microdomains, which can move laterally and coalesce into larger patches; thus, the association of a particular protein with these domains can result in its concentration and redistribution to specific subcellular structures (Mayor and Rao, 2004; Simons and Toomre, 2000). The polar distribution of specialized lipid domains within the plasma membrane has been implicated in polarized morphogenesis and motility in fungi and animals (Bagnat and Simons, 2002; Manes *et al.*, 2003; Martin and Konopka, 2004). Recent biochemical evidence has confirmed the presence of plasma membrane (PM) microdomains in plant cells, and has identified several sterols enriched in plant detergent-resistant membranes (DRMs), e.g. stigmasterol, sitosterol, 24-methyl-cholesterol, campesterol and cholesterol (Borner *et al.*, 2005; Mongrand *et al.*, 2004). Among these 3-β-hydroxysterols, stigmasterol and sitosterol have stronger abilities to promote micro-

domain formation than do common animal sterols such as cholesterol (Xu *et al.*, 2001). On the other hand, proteomic studies have revealed an enrichment of some polarity-related proteins in plant DRMs, such as SKU5 and COBRA, suggesting a role for these domains in the polar expansion of plant cells (Borner *et al.*, 2005; Mongrand *et al.*, 2004). Furthermore, the finding that polarized localization of the putative PM auxin transporter PIN1 is disrupted in the sterol-deficient Arabidopsis mutant *orc* demonstrated the potential importance of sterols in protein targeting, and thereby raised the possibility that sterol-rich microdomains may be involved in cell and tissue polarity in plants (Willemsen *et al.*, 2003). However, there is no direct evidence for a functional link between lipid microdomains and plant cell polar growth.

Early studies on lipid microdomains relied almost entirely on their purification as detergent-resistant membranes (Bhat and Panstruga, 2005; Chamberlain, 2004). In recent years, the emerging use of new fluorescent probes in combination with microscopy techniques provided a more direct way of detecting microdomains in living cells, by assessing membrane order rather than the enrichment of one lipid or protein species (Gaus *et al.*, 2003; Owen *et al.*, 2007). Di-4-ANEPPDHQ is a styryl dye newly introduced to image lipid microdomains in animal cells. The advantages over fluorescent protein-tagged microdomain-associated proteins and other popular phase-sensitive probes (e.g. Laurdan) make di-4-ANEPPDHQ an excellent probe for visualizing microdomains *in vivo* (Jin *et al.*, 2006; Owen *et al.*, 2006). The fluorescent sterol-binding antibiotic filipin has also has been used to visualize the polarization of PM microdomains in fungal and animal cells (del Pozo *et al.*, 2004; Takeda *et al.*, 2004), and was found to specifically bind 3-β-hydroxysterols in plants (Grebe *et al.*, 2003). On the other hand, incubation with high filipin concentrations and/or for an extended time-span has been shown to sequester sterols, disrupt PM microdomain structures and thereby impede microdomain-associated protein function (Papanikolaou *et al.*, 2005; Simons and Toomre, 2000; Wachtler *et al.*, 2003; Yang *et al.*, 2006). It thus remains unclear whether di-4-ANEPPDHQ can be applied to live plant cells to image PM microdomains, and whether the staining pattern coincides with that of filipin.

Tip-localized reactive oxygen species (ROS) production by PM NADPH oxidase (NOX, also termed Rboh in plants) is likely to be a general mechanism in the control of polarized growth of plant cells, such as pollen tubes, root hairs and Fucus zygotes (Carol *et al.*, 2005; Coelho *et al.*, 2008; Potocky *et al.*, 2007; Samaj *et al.*, 2004). NOX-derived ROS activate hyperpolarization-activated Ca^{2+} channels in the apical PM, which leads to Ca^{2+} influx, thus regulating a tip-focused Ca^{2+} gradient known to be essential for tip growth (Foreman *et al.*, 2003; Very and Davies, 2000). In this study, we used filipin, a sterol-chelating agent that disrupts microdomain structures, to explore the contribution of lipid microdomain polarization to the ROS-mediated polar growth in pollen tubes of *Picea meyeri*. Here, we show that NOX was partially included in low-density DRMs indicative of microdomain localization, and, furthermore, that superoxide production and pollen tube growth was inhibited by sterol sequestration. Moreover, we identified two distinct components of ROS production coexisting in actively growing pollen tubes.

RESULTS

Sterol-enriched membrane microdomains are polarized to pollen tube growing tips

To determine whether membrane lipids are polarized in healthy growing pollen tubes of *P. meyeri*, we grew tubes in culture medium (CM) for 18 h and stained them with the fluorescent probes filipin and di-4-ANEPPDHQ, respectively, to detect membrane heterogeneity. Staining with a low concentration (10 μM) of filipin revealed a clear gradient in plasma membrane labeling, with stronger fluorescence at the growing apex and much weaker fluorescence along the subapical flanks of pollen tubes (Figure 1a). A similar tip-localized pattern was also obtained when pollen tubes were stained with the phase-sensitive membrane dye di-4-ANEPPDHQ. This dye shows a large shift in its peak emission wavelength from ~630 nm in non-microdomain phase to ~570 nm in microdomain phase when bound to membranes, but very little fluorescence in water (Jin *et al.*, 2006). A normalized ratio of the two emission regions of di-4-ANEPPDHQ, displayed in pseudocolor, provided a relative measure of membrane order. Before the dye was added to the CM, no autofluorescence was detected when excited with the 488-nm laser line (Figure 1b; Video Clip S1). The dye readily inserted into the PM, and the fluorescence intensity increased to saturation level within 150 sec (Video Clip S1). In median confocal optical sections, di-4-ANEPPDHQ consistently produced a distinct peripheral and bright staining (Figure 1b). Tiny mobile fluorescent particles that likely represent the early endocytic vesicles progressively emerged in the apical cytoplasm, and then reached equilibrium. A representative ratio image showed that the lipid microdomains pseudocolored green to purple typically concentrated at the rapidly expanding region of the tube tip, where endocytosis and membrane trafficking actively occur (Figure 1b; Video Clip S1). It is important to note that these areas do not necessarily represent single lipid microdomains, but rather membrane domains in which the fraction of liquid-ordered phase is higher. Peripheral staining was shown to be associated with the plasma membrane, but not with the cell wall, as revealed by plasmolysis with 100 μM sorbitol in the presence of di-4-ANEPPDHQ (Figure S1a). Pre-treatment of pollen tubes with 500 μM sodium azide impaired dye uptake: di-4-ANEPPDHQ fluorescence could be observed only at the plasma membrane, and the dye was not internalized over time (Figure S1b).

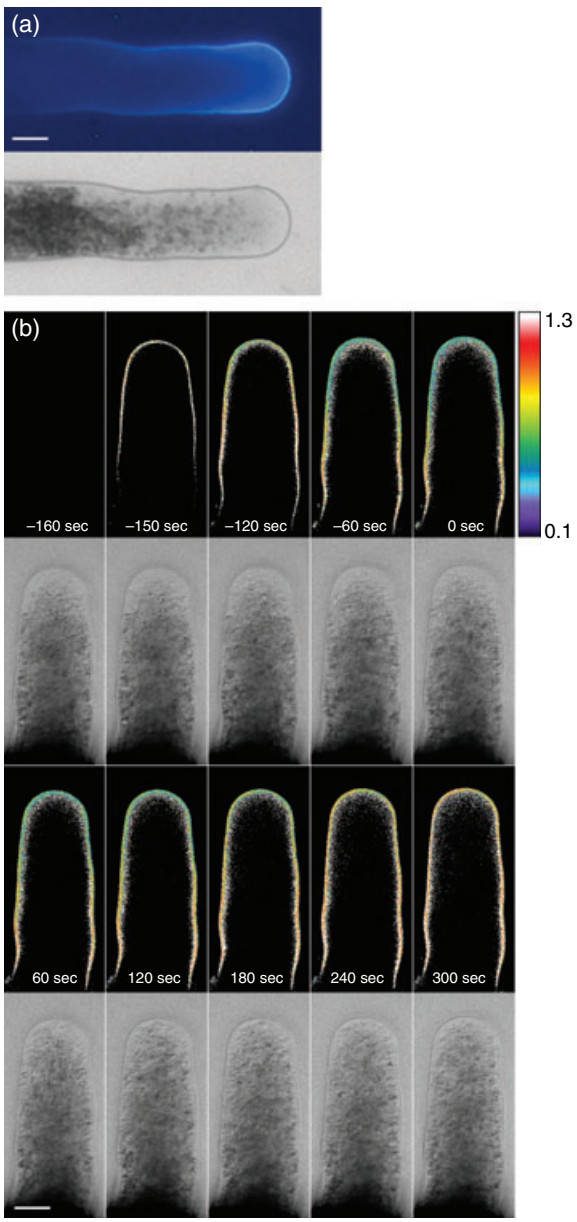

Figure 1. Sterol-enriched membrane polarization in growing *Picea meyeri* pollen tubes, and its relationship to sterol sequestration.
(a) Polarization of membrane sterols to the leading edge of growth during pollen tube elongation. The tubes were stained with a low concentration of filipin (10 μM) for 2 min and then analyzed by fluorescence microscopy. Scale bar: 10 μm.
(b) di-4-ANEPPDHQ uptake dynamics before (top panels) and fluorescence changes after (bottom panels) the addition of filipin. Times are relative to filipin addition, and di-4-ANEPPDHQ was added at −160 sec. For each time point, the ratio image (upper part) and bright field (lower part) are shown. The ratio images were pseudocolor-coded according to the inset scale, where blue to purple indicates a higher concentration of lipid microdomains. The full movie can be seen at Video Clip S1. Scale bar: 10 μm. For both experiments, images are representative of multiple experiments ($n > 5$).

To gain insight into the possible functions of lipid microdomains, we attempted to alter the structure of PM microdomains by incubation with filipin at a higher concentration. Extracellular perfusion of 20 μM filipin arrested pollen tube growth, whereas numerous small vacuole-like membranous structures (also called membranous tubules) migrated from the subapical region into the clear zone at the tip. Meanwhile, microdomain polarization was progressively shattered, and the membrane domains at the growing tip region became less ordered and more homogeneous (Figure 1b; Video Clip S1). This relatively high concentration is non-toxic to the cell, as suggested by the vigorous and steady cytoplasmic streaming in a typical fountain pattern during 5 min of incubation (Video Clip S1). Both fluorescein diacetate (FDA) and propidium iodide (PI) staining showed that even 8 min incubation with 20 μM filipin did not cause death to the *P. meyeri* pollen tubes (Figure S2); moreover, time-course analysis of confocal UV imaging and growth rate showed that after a thorough rinse, filipin-treated pollen tubes could internalize PM-inserted filipin by endocytosis, and then resumed polar tip growth, further indicating that 5 min of incubation with 20 μM filipin is mild, and that its effects are reversible (Figure S3).

Sterol sequestration attenuates tip-based ROS production and provokes the subapical ROS production

Nitroblue tetrazolium (NBT) was used to visualize the extracellular superoxide ($\cdot O_2^-$) production in tube cells. After a short incubation of 5 min, formazan deposit was typically formed most intensely at the growing tip of the control tubes (Figure 2a). In contrast, NBT staining in the apical PM was significantly decreased in pollen tubes pre-treated for 5 min with filipin (Figure 2b). The NOX inhibitor diphenylene iodonium (DPI) completely prevented the superoxide production, and no deposit was detected (Figure 2c): this result is consistent with the identification of NOX as the source of ROS production, which is essential for root hair growth (Carol *et al.*, 2005).

To examine the relative levels of endogenous ROS, we micro-injected tetramethylrhodamine dextran (10 000 MW) as a reference dye into the growing pollen tubes pre-loaded with CM-H_2DCFDA [5-(and-6)-chloromethyl-2′,7′-dichlorodihydrofluorescein diacetate, acetyl ester] and performed live cell time-lapse imaging. Oxidation of H_2DCF by ROS, principally by H_2O_2, yields the fluorescent DCF (Pei *et al.*, 2000). Ratiometric confocal images revealed intrinsic tip-based ROS production localized to the distal 10 μm of the normally growing apex, which was particularly noticeable at sites of membrane–cell wall adhesions (Figure 2d). The quantitative analysis of the corresponding fluorescence intensity revealed a steep ROS gradient with a sharply defined high signal in the extreme apex (Figure 2e). Beyond this region, however, another component of ROS production was also detectable in subapical regions (Figure 2d,e). The presence of 20 μM filipin induced a slight increase in tip-based ROS generation 60 sec after the addition of filipin, followed by an abrupt decrease at 120 sec, which then leveled off after

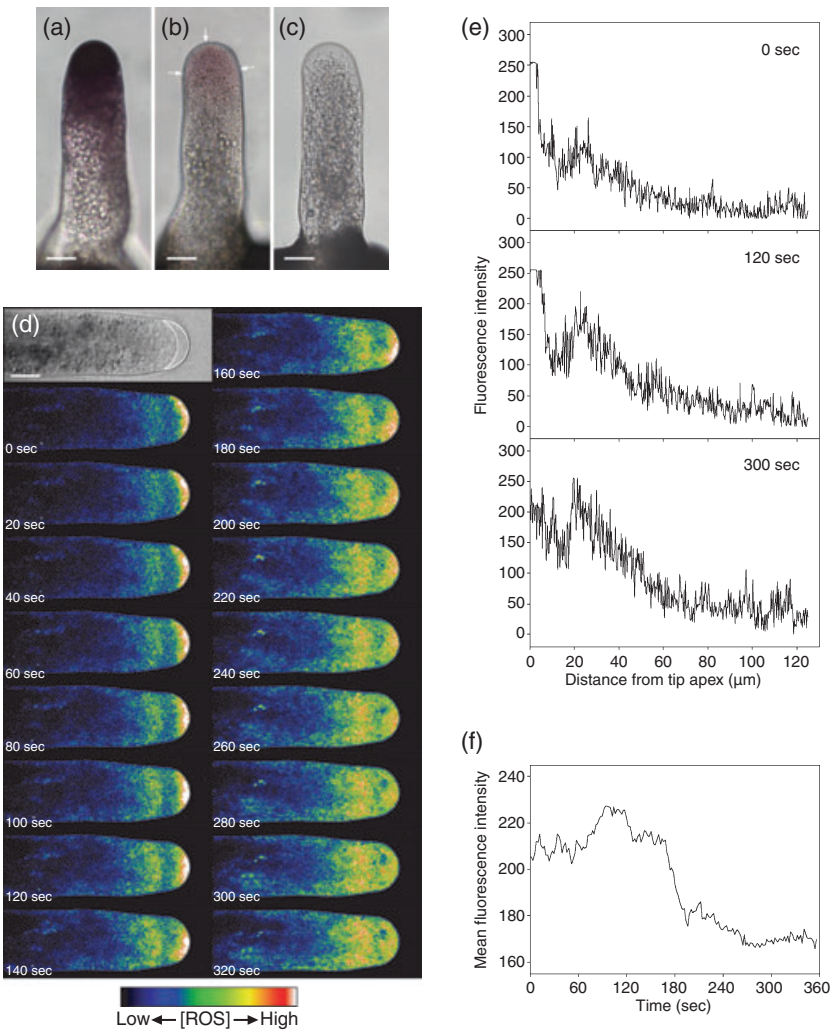

Figure 2. Sterol sequestration with a high filipin concentration depressed tip-based reactive oxygen species (ROS) production in growing *Picea meyeri* pollen tubes.
(a–c) Nitroblue tetrazolium (NBT) reduction detected extracellular tip-localized superoxide production in *P. meyeri* pollen tubes.
(a) Control tube showing intense formazan deposition at the growing tip.
(b) Much less deposit was observed when pre-incubated for 5 min and then stained in the presence of 20 μM filipin. Arrows indicate the site of NBT staining was the apical plasma membrane.
(c) The NADPH oxidase (NOX) inhibitor diphenylene iodonium (DPI) completely prevented extracellular superoxide production. Scale bars: 10 μm (a–c).
(d) Confocal time-lapse images of intracellular ROS production in response to filipin treatment. The ratio images were pseudocolor-coded according to the inset scale. Times are relative to filipin addition. The regions of interest (ROIs) outlined in the bright-field image (top left) mark the areas from which mean fluorescence was plotted in (f). Also see Video Clip S2. Scale bar: 20 μm.
(e) Comparison of the ROS fluorescence-intensity profile along the main axis of pollen tubes at 0 (left), 120 (middle) and 300 sec (right), showing clear spatial separation and temporal changes of the two components of ROS production.
(f) Time-lapse fluorescence intensity analysis of average ROS production in the apical region upon filipin treatment. Mean fluorescence (8-bit grey level value) was measured in the indicated ROIs in (d). For (a–d), the images are representative of at least five independent experiments.

260 sec (Figure 2d,f; Video Clip S2). In contrast to the overall decline shown for the apical ROS formation, the subapical ROS production steadily rose during filipin treatment. However, a gap between these two components was clearly present throughout the observation period, showing temporal separation of the ROS production in each region (Figure 2d,e; Video Clip S2). Meanwhile, numerous membranous tubules migrated from the region rich in amyloplasts into the tip, simultaneously with a progressive cessation of tube growth (Video Clip S2).

Sterol sequestration dissipates the tip-focused cytosolic Ca^{2+} gradient

We next asked whether cytosolic Ca^{2+} distribution was altered in filipin-treated tubes. Scanning confocal fluorescence microscopy of Calcium Green-1 is sufficient to show relative changes in Ca^{2+} concentration (Messerli *et al.*, 1999). Injection of growing tubes with Calcium Green-1 dextran revealed a typical tip-focused Ca^{2+} gradient extending from the tip to the base of the apical clear zone (Figure 3; Video Clip S3). Externally applied 20 μM filipin induced a dissipation of the apical Ca^{2+} gradient, with peak fluorescence falling rapidly after 180 sec (Figure 3; Video Clip S3). Finally, after approximately 300 sec, the Ca^{2+} gradient was almost completely dissipated, and only weak fluorescence was observed in the tip region.

NOX clusters correspond to ordered membrane domains of the growing tube tip

Because the foci of ROS production resulted from NOX activity (Foreman *et al.*, 2003; Potocky *et al.*, 2007; Takeda *et al.*, 2008), the similar polar distribution of ROS and ordered membrane domains led us to test whether lipid microdomains correlated with the spatial location of NOX. Control (Figure 4a–d) and filipin-treated (Figure 4e–h) pollen tubes were fixed and subjected to NOX immunolabeling, followed by di-4-ANEPPDHQ staining. The di-4-ANEPPDHQ staining showed that lipid microdomains in

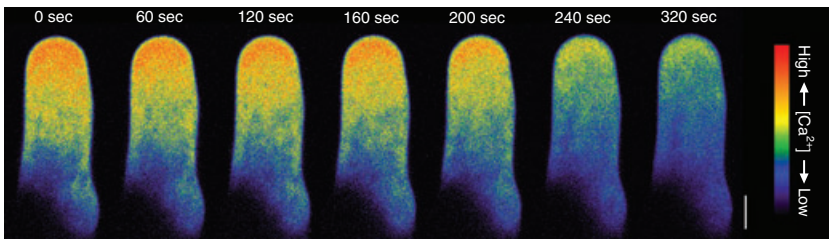

Figure 3. Confocal ratio images of a Ca^{2+} decrease in response to sterol sequestration.
The growing tube was microinjected with 2.5 mM Calcium Green-1 dextran and then subjected to filipin treatment. The images were pseudocolor-coded according to the inset scale. Times are relative to filipin addition. Also see Video Clip S3. Images are representative of multiple experiments (n = 7). Scale bar: 20 μm.

Figure 4. Ratio and immunofluorescence images of control and filipin-treated pollen tubes.
Control (a–d) and filipin-treated (e–h) pollen tubes attached to coverslips were fixed, immunostained and di-4-ANEPPDHQ labeled as described in Experimental procedures. Ratio images (a) and (e) were calculated and pseudocolored as for Figure 1. Panels (b) and (f) show the corresponding confocal images of NADPH oxidase (NOX) immunostaining; panels (c) and (g) show ratio values of NOX-stained pixels. The regions of interest (ROIs) outlined in (c) and (g) were magnified, rotated 90° clockwise and are shown in (d) and (h). Scale bars: 10 μm (c, g); 2 μm (d, h).

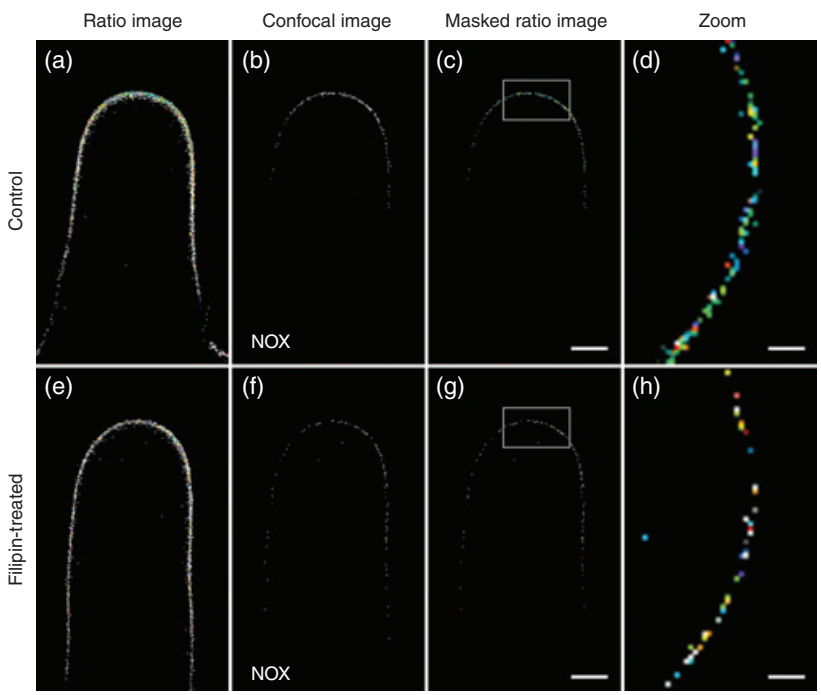

the fixed control cells were similarly localized to the growing tip, as in the living tubes, but with fewer particles in the cytoplasm (Figure 4a). Staining with antibodies against the putative MtRboh revealed that NOX almost exclusively accumulated in clusters in the apical PM region of pollen tubes (Figure 4b). Figure 4c showed the masked ratio images of NOX in control tubes. Particularly when magnified (Figure 4d), it became apparent that NOX-stained pixels were substantially enriched in low-ratio value areas, colored green to purple. However, some NOX clusters did not correspond to particular ordered membrane domains. While in the filipin-treated pollen tubes, the membrane heterogeneity along the tube was almost abolished (Figure 4e), and the NOX stain spread to the flanks of pollen tubes in a dispersed manner (Figure 4f). As shown in Figure 4h at a higher magnification of the masked ratio images (Figure 4g), NOX-positive regions corresponded to less ordered membrane domains.

NOX is partially associated with flotillin-1-enriched DRMs of pollen tubes

To verify the NOX localization to lipid microdomains of pollen tubes, we applied the standard Triton X-100 extraction protocol on purified PM fractions to isolate DRMs in a 5:20:25% discontinuous Optiprep density flotation gradient. Six fractions were analyzed for total proteins and sterols (Figure 5a). Relatively little protein was present in the light/DRM fractions (fractions 2–3, corresponding to the 5/20% interface), whereas the bulk of the proteins was found in the dense fractions, as generally reported. Conversely, sterol levels were high in the DRM fractions (~190 μg sterol mg $protein^{-1}$) compared with the high-density fractions (15–30 μg sterol mg $protein^{-1}$). These properties are typical characteristics of plant DRMs (Borner *et al.*, 2005). We further characterized these fractions by immunoblotting using antibodies against NOX and the known plant

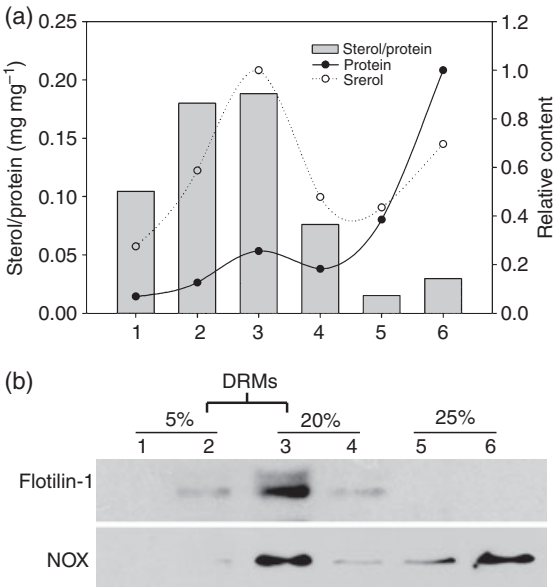

Figure 5. NADPH oxidase (NOX) partially associates with non-ionic detergent extracts of pollen tubes. detergent-resistant membranes (DRMs) were isolated by density gradient centrifugation after membrane extraction with cold 1% Triton X-100.
(a) Distributions of sterols and proteins and their ratios across the Optiprep step gradient. Protein and sterol contents of each fraction were determined and normalized to 1, according to their respective maximal values.
(b) Western blots showing the distribution of flotillin-1 and NOX along the Optiprep density gradients after extraction of purified plasma membrane (PM) on ice with Triton X-100. NOX co-migrated with the microdomain markers in light fractions 2–3 (5/20% interface). Substantial quantities of NOX were also recovered in the heavy fractions at the bottom of the gradient.

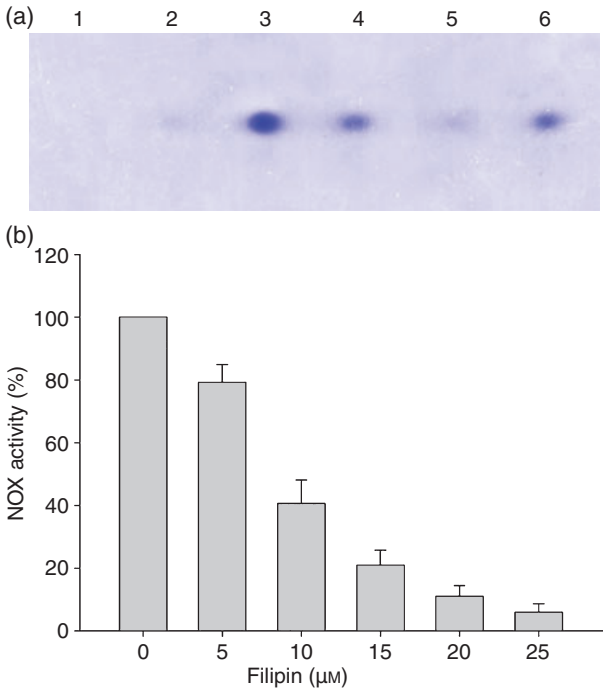

Figure 6. NADPH oxidase (NOX) enzymatic activity is detergent-resistant membranes (DRM)-associated and sterol-dependent.
(a) *In situ* gel nitroblue tetrazolium (NBT) assay for NOX activity in the various fractions collected from the Optiprep gradients. Protein samples from each fraction (50 μl per lane) were separated in a native gel at 4°C. The gel was incubated with NBT for 20 min, and then with NADPH until the appearance of blue formazan bands was observed.
(b) The enzymatic activity of NOX is inhibited by treatment of DRMs with filipin in a dose-dependent manner. *Picea meyeri* pollen tube DRMs (fraction 3) were incubated with the indicated concentrations of filipin at room temperature for 10 min with agitation. The superoxide-producing capabilities of the samples were measured based on 2,3-bis-(2-methoxy-4-nitro-5-sulfophenyl)-2*H*-tetrazolium-5-carboxanilide (XTT) reduction. Data are given as percentages of the activity of the control sample ± SEs of six replicates.

microdomain protein flotillin-1 (Borner *et al.*, 2005). As shown in Figure 5b, flotillin-1 was recovered almost exclusively in fractions 2–3, as expected for DRMs. Furthermore, light fractions, which displayed canonical biochemical properties of lipid microdomains, contained significant quantities of NOX. Substantial quantities of NOX were also recovered in the heavy fraction 6 at the bottom of the gradient. Together, the biochemical analysis of DRMs clearly suggested the inclusion of NOX into lipid microdomains.

NOX requires sterol-based microdomain association for enzymatic activity

To test whether the NOX activity is present in DRMs, we carried out an *in situ* gel NBT assay on DRMs of pollen tubes. Protein samples from each fraction were separated by 7.5% non-denaturing PAGE, and NBT staining was performed in gel. As shown in Figure 6a, a main activity band was detected in native gels in fraction 3, corresponding to DRMs, which overlapped with the cross-reactivity band with the antibody against MtRboh. Only weak bands were observed in non-DRM fractions 4 and 6, even in the presence of NOX. Based on these results, we examined whether sterol sequestration has functional significance for NOX enzymatic activity in DRMs. Incubation of isolated DRMs (fraction 3) with 2,3-bis-(2-methoxy-4-nitro-5-sulfophenyl)-2*H*-tetrazolium-5-carboxanilide (XTT) gave rise to a water-soluble blue formazan product, confirming the enzymatic activity in PM microdomains. Measurement of the XTT formazan concentration showed that filipin treatment resulted in the dramatic inhibition of superoxide-producing activity in a dose-dependent manner (Figure 6b). The concentration of filipin required to inhibit NOX activity by 80% was estimated at 15.6 μM.

DISCUSSION

Lipid microdomain polarization is associated with pollen tube apical growth

Lipid microdomains are highly dynamic entities floating freely in the surrounding membranes of living cells (Simons and Toomre, 2000). By clustering small individual microdomains into a larger platform, certain microdomain-associated signaling proteins are recruited together for

modification, allowing foci for signal transduction to be assembled in physiological conditions (Ikonen, 2001). In the fungal pathogen *Candida albicans*, for example, a dramatic polarization of lipid microdomains to the hyphal tip was observed during all stages of hyphal growth, which shares most of the features common to tip-growing plant cells such as root hairs and pollen tubes (Martin and Konopka, 2004). In this study, a new styryl dye di-4-ANEPPDHQ was successfully applied in plants, and the polarization of PM microdomains to the growing tip of a pollen tube was visualized *in vivo*. Experiments of plasmolysis with sorbitol and the effect of sodium azide on di-4-ANEPPDHQ uptake (Figure S1) demonstrated that dye staining was in the plasma membrane rather than the cell wall, and that dye internalization occurred via an endocytic mechanism rather than passive diffusion. Moreover, the di-4-ANEPPDHQ staining pattern was consistent with results obtained with the sterol-binding antibiotic filipin (Figure 1). Filipin fluorescence at the tube apex indicated an enrichment of 3-β-hydroxysterols, a typical feature of plant DRMs (Bhat *et al.*, 2005; Borner *et al.*, 2005; Mongrand *et al.*, 2004). The similar localization pattern of membrane sterol and microdomains clearly implied the involvement of sterol-enriched lipid microdomains in tube polar growth.

Sterol sequestration elicits a different response of cytoplasmic ROS components

The ROS produced by NOX have been proposed to modulate root hair polar growth by activating a Ca^{2+} channel required to generate the tip-focused Ca^{2+} gradient (Carol *et al.*, 2005; Foreman *et al.*, 2003; Samaj *et al.*, 2004; Takeda *et al.*, 2008). In this study, both NBT reduction and H_2DCF oxidation revealed that tip-based ROS production is indeed present in the actively growing apical region, highlighting the reported signaling role for ROS in polar cell growth (Coelho *et al.*, 2008; Foreman *et al.*, 2003; Takeda *et al.*, 2008). This is further supported by our observation that the attenuated apical ROS production caused by sterol sequestration inevitably dissipated the apical Ca^{2+} gradient, leading to the accumulation of vesicles and vacuolation at tube tips, which eventually arrested polar growth (Video Clips S1–S3). A positive feedback loop by the local interaction of ROS and Ca^{2+} was recently reported to be central to the maintenance of polarized cell growth (Takeda *et al.*, 2008; Wong *et al.*, 2007). Accordingly, the dissipated Ca^{2+} concentration may, in turn, have aggravated the decline in the apical ROS production in this study. Furthermore, another ROS component was identified as being located in the subapical region, which is clearly separated from the apical component. Given the fact that the intracellular generation of ROS is an inevitable byproduct of mitochondrial energy metabolism (Coelho *et al.*, 2002), the steady rise of ROS during filipin treatment may be a response to sterol sequestration, and will be most concentrated in the region where mitochondria usually accumulate in pollen tubes. Our observation is consistent with an earlier report that ROS production associated with mitochondrial metabolism is detected in subapical regions of actively growing lily pollen tubes (Cardenas *et al.*, 2006). Thus, our study provides strong evidence for the coexistence of these two distinctly different ROS components during normal pollen tube growth.

Microdomain association is required for NOX clustering and enzymatic activity

ROS are diffusible and short-lived molecules, and therefore localizing the NOX-derived ROS signal precisely is essential for growth control (Foreman *et al.*, 2003). Immunolocalization in this study showed that NOX clustered to the growing tip of pollen tubes, as in elongating Arabidopsis hairs (Takeda *et al.*, 2008), and this localization restricts ROS production to the growth points during cell elongation. In animal cells, ROS production may be localized through interactions of NOX with signaling platforms associated with lipid microdomains (Vilhardt and van Deurs, 2004). Here, the overlapping of NOX stain with low ratio value areas indicated that NOX may reside in lipid microdomains. To ascertain this localization, we isolated lipid microdomains with Optiprep gradients after the solubilization of PMs by Triton X-100, and found that NOX was partially included in the low-density fractions, together with the plant microdomain marker flotillin-1, confirming the inclusion of NOX into lipid microdomains. This result is consistent with the recent report that this enzyme was immunologically detected in tobacco DRMs upon cryptogein elicitation (Mongrand *et al.*, 2004). Furthermore, sterol sequestration by filipin greatly weakened the membrane heterogeneity, disrupted the polar localization of NOX, and NOX-positive regions became less ordered after filipin treatment, further suggesting that sterol-based microdomain association tends to concentrate NOX within ordered membrane domains in the apical PM. On the other hand, in-gel assays showed that NOX depends on the microdomain environment for enzymatic activity, and interference with membrane sterols with increasing filipin levels resulted in a substantial decrease in the enzymatic activity of NOX in DRMs. These data suggest that the activity of NOX, the microdomain-localized ROS-producing enzyme essential for polarized tube growth, is DRM-associated and sterol-dependent.

It is becoming more evident that Rho-like small GTPases of plants (ROPs) might function as a positive regulator of NOX to regulate spatially controlled ROS production and Ca^{2+} distribution (Jones *et al.*, 2002; Wong *et al.*, 2007). Upon GTP binding and activation, ROPs are transiently S-acylated, which induces their partitioning into DRMs (Sorek *et al.*, 2007). The concomitant recruitment of NOX and ROPs to lipid microdomains reinforces the putative role of these microdomains during the plant defense response (Mittler *et al.*, 2004; Mongrand *et al.*, 2004). Furthermore,

localization of activated ROP GTPases to the apical membrane is associated with the tip-growing pollen tubes (Gu *et al.*, 2005; Hwang *et al.*, 2005; Lin and Yang, 1997). Accordingly, we propose that as in normal cell growth, microdomain binding recruits NOX and ROPs to a preferable micro-environment for their efficient coupling, and thus warrant a high ROS-producing activity of NOX, which enables a polarized tip growth in pollen tubes. Our observation that sterol sequestration by filipin disrupted microdomain polarization, depressed enzymatic activity of NOX, and thus dissipated the apical Ca^{2+} gradient is indeed consistent with such a hypothesis. Furthermore, it should be noted that the anti-NOX antibody used here was raised against the conservative C-terminal domain of the putative *Medicago truncatula* Rboh protein. The NCBI Blast results showed that the antigen peptide sequence could be found in other plant respiratory burst oxidase homologs or plant respiratory burst oxidase-like proteins, and these defined proteins containing this sequence were all associated with the rapid release of ROS. Although there is now a deficiency in the conifer NOX gene data, the immunological tests indicated the presence of NOX protein in *P. meyeri*. However, whether *P. meyeri* has a NOX gene family and which isoform is involved in pollen tube tip growth remain to be further explored.

In summary, our investigations of the effects of sterol sequestration on *P. meyeri* pollen tubes have provided a more global view on the roles of lipid microdomains in polarized tip growth in pollen tubes. Based on biochemical and biophysical evidence, a hypothetical model for a functional link between sterol-rich PM microdomains and the ROS-producing activity of NOX in pollen tubes is proposed in Figure 7. This study provides two novel findings in plant cells: (i) the association of NOX with polarized lipid microdomains could be involved in its targeting to the apical PM region; (ii) NOX requires sterol-based microdomain association for enzymatic activity. Data presented here demonstrate that the polarization of lipid microdomains to the apical PM, and the inclusion of NOX, a crucial growth regulator, into these domains contribute, at least in part, to the ability to grow in a highly polarized manner to form pollen tubes.

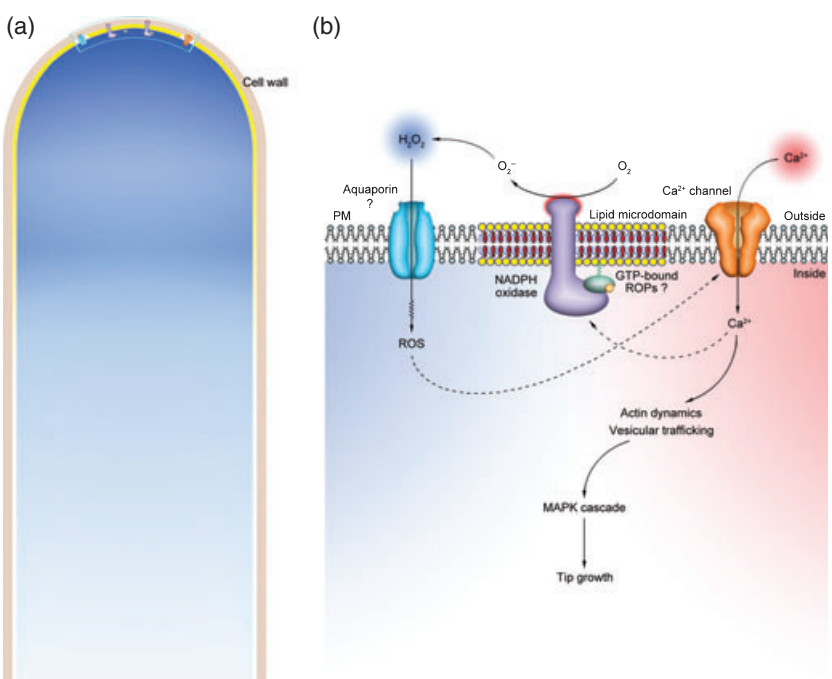

Figure 7. Hypothetical model of lipid microdomain polarization involved in the spatial regulation of NADPH oxidase (NOX) activity in *Picea meyeri* pollen tube tip growth.

(a) Lipid microdomains cluster at the growing tip region, and thus the association of NOX and Rho-like small GTPases of plants (ROPs) with microdomains result in their concentration and efficient coupling in the apical plasma membrane (PM), thereby activating NOX enzymatic activity. The subapical component of intracellular reactive oxygen species (ROS) production associated with mitochondrial metabolism is also shown. Note that bright yellow represents membrane domains in which the fraction of the liquid-ordered phase is higher.

(b) Magnified view of the boxed region in (a). Detergent-resistant membrane (DRM)-localized NOX catalyzes the extracellular formation of superoxide anion ($\cdot O_2^-$), which is rapidly converted to H_2O_2 and OH·(Van Breusegem *et al.*, 2008). H_2O_2 readily crosses the PM through specific aquaporins (Henzler and Steudle, 2000). The localized increase in intracellular ROS activates the apical Ca^{2+} channels, leading to the establishment of a tip-focused Ca^{2+} gradient known to regulate cytoskeletal rearrangements and vesicular trafficking, which are essential for plant cell polar growth. In turn, Ca^{2+} binding enhances NOX activity, forming a positive feedback loop to reinforce this polarity (Takeda *et al.*, 2008). The ROS gradient is depicted in blue, whereas the Ca^{2+} gradient is depicted in red. Question marks indicate that the identity of these putative proteins has not been confirmed, and dashed arrows indicate unidentified signaling pathways in *P. meyeri*.

EXPERIMENTAL PROCEDURES

Antibodies and reagents

The anti-NOX polyclonal antiserum was raised in rabbits against the conservative C-terminal domain of the putative MtRboh protein (amino acids 702–716, CAM35833). The rabbit polyclonal anti-flotollin-1 antibody was prepared against full-length Arabidopsis flotillin-1 (AtFlot1; At5g25250). CM-H_2DCFDA, di-4-ANEPPDHQ, Calcium Green-1 dextran (10 000 MW), tetramethylrhodamine dextran (10 000 MW), and Cy3-conjugated goat anti-rabbit IgG antibody were purchased from Invitrogen (http://www.invitrogen.com). Filipin III, NBT, DPI, XTT, cellulase, pectinase, plant protease inhibitor cocktail and other chemicals were from Sigma-Aldrich (http://www.sigmaaldrich.com). To prepare stock solutions, filipin III and di-4-ANEPPDHQ were dissolved in ethanol, whereas CM-H_2DCFDA, NBT and DPI were dissolved in anhydrous DMSO (<0.05% final concentration).

Pollen tube culture

For biochemical studies, pollen grains (100 mg) of *P. meyeri* Rehd. et Wils. were germinated and grown at 24–26°C in 100 ml of culture medium containing 1 mM H_3BO_3, 1 mM $CaCl_2$ and 350 mM sucrose. For fluorescence studies, germinated pollen tubes were plated on a coverslip forming the bottom of an open-top slide chamber, with a thin layer of CM supplemented with 0.7% (w/v) Sigma type-VII low gelling point agarose (Cardenas *et al.*, 2006; Lin and Yang, 1997). The gelled agarose should be as thin as possible to keep the tubes flat, and as close to the coverslip as possible. Following 2 h recovery, the agarose was carefully removed from near the tube tip, the exposed surface covered with CM, and the tube was allowed to grow out of the cut surface. After ~7 h of growth when the tubes were 80–100 μm in length, the CM was supplemented with various stock solutions for treatment.

Filipin staining and sterol sequestration

Filipin treatments were performed based on the methods of Wachtler *et al.* (2003) and Grebe *et al.* (2003). Pollen tubes were mounted on the microscope stage, and a 1 mM stock solution of filipin III in ethanol was added to the CM held in the slide chamber. For staining purposes, filipin III was used at a final concentration of 10 μM (6.6 μg ml^{-1}) and then observed immediately with a Zeiss Axioskop 40 microscope (http://www.zeiss.com) fitted with a Qimaging Retiga 1300 12-bit monochrome CCD camera. Filipin treatment for disruption of sterol-rich membrane domains was carried out at 25°C by incubation for 5 min with filipin III at a relatively high concentration of 20 μM (13.1 μg ml^{-1}). The cell vitality was examined by FDA staining and PI staining. For recovery experiments, the filipin-containing treatment solution was gently replaced with drug-free CM. Filipin was excited with a 405-nm laser, and fluorescence was observed between 470 and 490 nm by using a Leica TCS-SP5 CLSM (http://www.leica-microsystems.com).

Imaging of membrane microdomains

Di-4-ANEPPDHQ staining was performed by adding 5 μM di-4-ANEPPDHQ to the CM before inhibitory filipin incubation. Pollen tubes were imaged with a Zeiss LSM 510 META confocal microscope by using a ×63 water-immersion, 1.2 N.A., C-Apochromat objective. The fluorescence is excited by the 488-nm argon laser, and is collected simultaneously through long pass (LP) 650-nm and band-pass (BP) 505–550-nm filters. Bright-field images were acquired simultaneously by using the transmission detector. For time-lapse analysis under control conditions and after filipin addition, individual images were captured every 5 sec. Ratio images are calculated by dividing the emission intensity from the LP 650-nm channel by that from the BP 505–550-nm channel on a pixel-by-pixel basis using MetaMorph imaging software (http://www.universalimaging.com), according to the method described by Jin *et al.* (2006).

Extra- and intracellular ROS detection

To visualize the extracellular release of ROS (mainly superoxide anion, O_2^-) around the exposed pollen tubes, NBT staining was performed as described in Carol *et al.* (2005). Control or filipin-treated (5 min) tubes were incubated for 5 min with 0.1% NBT in CM, and were imaged under bright-field illumination on the Zeiss Axioskop 40 microscope. Negative control experiments were performed by growing pollen tubes in CM containing 50 μM DPI (30 min), and then staining them in identical medium with 1 mg ml^{-1} NBT added (5 min).

The intracellular distribution of ROS was determined as described in Cardenas *et al.* (2006). For ratiometric confocal ROS imaging, agarose-embedded pollen tubes were first pressure injected with 5 mM tetramethylrhodamine dextran (10 000 MW) on a Zeiss Axiovert 200M inverted microscope. Following the removal of the needle and complete recovery, the pollen tubes were incubated for 20 min with 20 μM CM-H_2DCFDA, and then rinsed with dye-free CM. Image pairs were acquired with the Zeiss LSM 510 META microscope. First, we excited CM-H_2DCFDA with the 488-nm argon laser, and then collected the emission through a 500–550-nm BP filter. Second, tetramethyl-rhodamine dextran (10 000 MW) was excited with the 543-nm HeNe laser, and the emission was collected through a 560-nm LP filter. A ratio of these two signals permitted us to map out the relative levels of ROS in the pollen tube. Time-lapse image pairs were collected at 10-sec intervals, with DIC images acquired simultaneously. The fluorescence intensity for ROS production was plotted versus relative distances from the tip apex to the base along the main axis of pollen tubes.

Imaging of cytosolic Ca^{2+} levels

To image cytoplasmic Ca^{2+}, growing pollen tubes were injected with 2.5 mM Calcium Green-1 linked to a 10-kDa dextran. Following the removal of the needle and the complete recovery from the injection, the tubes were imaged with the same microscope and imaging parameters as described above for DCF. Fluorescent images were captured with DIC images at 20-sec intervals for up to 5 min.

Immunofluorescence co-localization

Pollen tubes were fixed at room temperature (25°C) for 1 h with 4% paraformaldehyde in CM. After extensive rinsing in phosphate-buffered saline (PBS; pH 6.8), the cell walls of pollen tubes were digested with 1% cellulase and 1% pectinase in PBS (pH 5.8) for 20 min. Samples were then permeabilized and blocked in PBS (pH 7.5) containing 0.5% Triton X-100, 1% BSA, and then incubated at 37°C for 1 h each with primary rabbit polyclonal anti-MtRboh (1:200 dilution) and secondary Cy3-conjugated goat anti-rabbit IgG antibody (1:800 dilution), and were then thoroughly washed after each incubation period. Afterwards, the samples were stained with di-4-ANEPPDHQ in PBS, covered with a drop of 10% (v/v) glycerol in PBS, and then viewed under the Zeiss LSM 510 META confocal microscope. To correlate di-4-ANEPPDHQ ratio values with NOX clusters, we used the immunofluorescent images to mask the ratio images: the masked ratio images only show the immunostained pixels, using the same pseudocoloring to indicate ratio values.

Biochemical lipid microdomain separation

Cell membranes (microsomal fractions) were prepared from cultured pollen tubes according to (Sun *et al.*, 2000). PM fractions were isolated from microsomes by two-phase partitioning with 6.4% (w/w) dextran T-500 and 6.4% (w/w) PEG 3350, as described in Sagi and Fluhr (2001). DRMs were prepared by low-temperature detergent extraction, adapting the protocol described in Bagnat *et al.* (2000). Briefly, PMs (~2 mg) were resuspended in 1 ml ice-cold TE buffer (25 mM Tris–HCl, 5 mM EDTA, pH 7.5) containing protease inhibitors and 1% Triton X-100. Extractions were carried out on ice shaking at 100 rpm for 30 min. Thereafter, the extracts were placed at the bottom of a centrifuge tube, mixed with Optiprep solution (Nycomed, http://www.nycomed.com) to make 2 ml, with a final concentration of 25%, and overlain with 2 ml of 20% Optiprep in TE and 2 ml of 5% Optiprep in TE. The samples were centrifuged at 51 400 ***g*** for 3 h in a Beckman SW41 Ti rotor at 4°C, and six fractions of equal volume (1 ml) were harvested from the tops of the gradients.

Quantification of sterols and proteins

For sterol determination, the membrane samples from each fraction were saponified by refluxing for 2 h with 1 N ethanolic KOH. The non-saponifiable fraction containing total sterols were extracted into diethyl ether, and the ethereal extract was evaporated to dryness. The total sterol content was determined on the residue by the Liebermann–Burchard color reaction. A standard curve was constructed using a sample of cholesterol. The protein level of each fraction was measured by using a bicinchoninic acid protein assay kit (Pierce, http://www.piercenet.com) to avoid Triton X-100 interference. To solubilize membrane proteins, assays were carried out in the presence of 2–3% SDS.

Western blot analysis

SDS-PAGE and western analysis were performed using the standard Laemmli method. Proteins from each fraction were incubated with sample buffer at 60°C for 5 min, loaded into a 7.5% (w/v) polyacrylamide gel (Mini-Protean II; Bio-Rad, http://www.bio-rad.com), electrophoresed, and then finally electrotransferred onto a nitrocellulose membrane. For immunodetection, blotted membranes were incubated with primary antibodies specific for the NOX (polyclonal, 1:2000 dilution) or the flotillin-1 (monoclonal, 1:5000 dilution). Immunoblots were visualized by using the appropriate HRP-conjugated secondary antibody (1:5000 dilution for goat anti-rabbit; 1:2000 dilution for goat anti-mouse) and the enhanced chemiluminescence detection system (Amersham Biosciences, now part of GE Healthcare, http://www.gehealthcare.com).

In situ gel NBT assay

The superoxide-producing capability of NOX was assayed in native gels by a modified NBT reduction method (Sagi and Fluhr, 2001). Protein samples from each fraction (10 μl per lane) were separated in a 6% (w/v) non-denaturing polyacrylamide gel with 0.1% (v/v) CHAPS at 4°C. The gel was incubated in the dark with 0.2 mM NBT solution (50 mM Tris–HCl, 0.2 mM NBT, 0.1 mM $MgCl_2$, and 1 mM $CaCl_2$, pH 7.4) for 20 min, and then with 0.5 mM NADPH until the appearance of blue formazan bands was observed. The reaction was stopped by immersion of the gel in distilled water.

Sterol-dependent NOX activities assays

NOX activities were assayed in the DRMs fraction based on the reduction of XTT by $\cdot O_2^-$ radicals (Able *et al.*, 1998). The reaction mixture contained 0.3 mM XTT, 20 mM Tris–HCl (pH 7.4), and a 20 μl of fraction 3 with varying concentrations of filipin (0–25 μg ml^{-1}) in a total volume of 0.5 ml. The reaction was initiated in a microcuvette at room temperature by the addition of NADPH, and was scanned by the change in A470 over 5 min in a spectrophotometer (DU 640; Beckman Coulter, http://www.beckman.com).

ACKNOWLEDGEMENTS

We thank Danying Lin (Tsinghua University, China) and Wei Zhang (Institute of Chemistry, Chinese Academy of Sciences) for their generous help on data processing and manuscript correction. This work was funded by National Key Basic Research Program (2007CB108703, 2006CB910606 and 2009CB119105) from MOST, a key project from NSFC (30730009), and a grant from Deutsche Forschungsgemeinschaft to JŠ (DFG, SA 1564/2-1).

SUPPORTING INFORMATION

Additional Supporting Information may be found in the online version of this article:

Figure S1. Effects of plasmolysis and sodium azide on di-4-ANEPPDHQ uptake.

Figure S2. Fluorescein diacetate (FDA) staining and propidium iodide (PI) staining of the filipin-treated pollen tubes.

Figure S3. Time-course analysis of filipin fluorescence and pollen tube growth rate in response to filipin addition and wash-out.

Video Clip S1. Development and changes of di-4-ANEPPDHQ fluorescence with time, before and after the addition of filipin.

Video Clip S2. Dynamic changes of intracellular reactive oxygen species (ROS) production, as reported by DCF in response to filipin treatment.

Video Clip S3. Sterol sequestration dissipated the tip-focused cytoplasmic Ca^{2+} gradient.

Please note: Wiley-Blackwell are not responsible for the content or functionality of any supporting materials supplied by the authors. Any queries (other than missing material) should be directed to the corresponding author for the article.

REFERENCES

Able, A.J., Guest, D.I. and Sutherland, M.W. (1998) Use of a new tetrazolium-based assay to study the production of superoxide radicals by tobacco cell cultures challenged with avirulent zoospores of phytophthora parasitica var nicotianae. *Plant Physiol.* **117**, 491–499.

Bagnat, M. and Simons, K. (2002) Cell surface polarization during yeast mating. *Proc. Natl Acad. Sci. USA*, **99**, 14183–14188.

Bagnat, M., Keranen, S., Shevchenko, A., Shevchenko, A. and Simons, K. (2000) Lipid rafts function in biosynthetic delivery of proteins to the cell surface in yeast. *Proc. Natl Acad. Sci. USA*, **97**, 3254–3259.

Bhat, R.A. and Panstruga, R. (2005) Lipid rafts in plants. *Planta*, **223**, 5–19.

Bhat, R.A., Miklis, M., Schmelzer, E., Schulze-Lefert, P. and Panstruga, R. (2005) Recruitment and interaction dynamics of plant penetration resistance components in a plasma membrane microdomain. *Proc. Natl Acad. Sci. USA*, **102**, 3135–3140.

Borner, G.H., Sherrier, D.J., Weimar, T., Michaelson, L.V., Hawkins, N.D., Macaskill, A., Napier, J.A., Beale, M.H., Lilley, K.S. and Dupree, P. (2005) Analysis of detergent-resistant membranes in Arabidopsis. Evidence for plasma membrane lipid rafts.. *Plant Physiol.* **137**, 104–116.

Cardenas, L., McKenna, S.T., Kunkel, J.G. and Hepler, P.K. (2006) NAD(P)H oscillates in pollen tubes and is correlated with tip growth. *Plant Physiol.* **142**, 1460–1468.

Carol, R.J., Takeda, S., Linstead, P., Durrant, M.C., Kakesova, H., Derbyshire, P., Drea, S., Zarsky, V. and Dolan, L. (2005) A RhoGDP dissociation inhibitor spatially regulates growth in root hair cells. *Nature*, **438**, 1013–1016.

Chamberlain, L.H. (2004) Detergents as tools for the purification and classification of lipid rafts. *FEBS Lett.* **559**, 1–5.

Coelho, S.M., Taylor, A.R., Ryan, K.P., Sousa-Pinto, I., Brown, M.T. and Brownlee, C. (2002) Spatiotemporal patterning of reactive oxygen

production and Ca^{2+} wave propagation in Fucus rhizoid cells. *Plant Cell*, **14**, 2369–2381.

Coelho, S., Brownlee, C. and Bothwell, J. (2008) A tip-high, Ca^{2+}-interdependent, reactive oxygen species gradient is associated with polarized growth in Fucus serratus zygotes. *Planta*, **227**, 1037–1046.

Foreman, J., Demidchik, V., Bothwell, J.H.F. *et al.* (2003) Reactive oxygen species produced by NADPH oxidase regulate plant cell growth. *Nature*, **422**, 442–446.

Gaus, K., Gratton, E., Kable, E.P.W., Jones, A.S., Gelissen, I., Kritharides, L. and Jessup, W. (2003) Visualizing lipid structure and raft domains in living cells with two-photon microscopy. *Proc. Natl Acad. Sci. USA*, **100**, 15554–15559.

Grebe, M., Xu, J., Mobius, W., Ueda, T., Nakano, A., Geuze, H.J., Rook, M.B. and Scheres, B. (2003) Arabidopsis sterol endocytosis involves actin-mediated trafficking via ARA6-positive early endosomes. *Curr. Biol.* **13**, 1378–1387.

Gu, Y., Fu, Y., Dowd, P., Li, S., Vernoud, V., Gilroy, S. and Yang, Z. (2005) A Rho family GTPase controls actin dynamics and tip growth via two counteracting downstream pathways in pollen tubes. *J. Cell Biol.* **169**, 127–138.

Henzler, T. and Steudle, E. (2000) Transport and metabolic degradation of hydrogen peroxide in Chara corallina: model calculations and measurements with the pressure probe suggest transport of H_2O_2 across water channels. *J. Exp. Biol.* **51**, 2053–2066.

Hwang, J.-U., Gu, Y., Lee, Y.-J. and Yang, Z. (2005) Oscillatory ROP GTPase activation leads the oscillatory polarized growth of pollen tubes. *Mol. Biol. Cell*, **16**, 5385–5399.

Ikonen, E. (2001) Roles of lipid rafts in membrane transport. *Curr. Opin. Cell Biol.* **13**, 470–477.

Jin, L., Millard, A.C., Wuskell, J.P., Dong, X., Wu, D., Clark, H.A. and Loew, L.M. (2006) Characterization and application of a new optical probe for membrane lipid domains. *Biophys. J.* **90**, 2563–2575.

Jones, M.A., Shen, J.-J., Fu, Y., Li, H., Yang, Z. and Grierson, C.S. (2002) The Arabidopsis Rop2 GTPase is a positive regulator of both root hair initiation and tip growth. *Plant Cell*, **14**, 763–776.

Lin, Y. and Yang, Z. (1997) Inhibition of pollen tube elongation by microinjected anti-Rop1Ps antibodies suggests a crucial role for Rho-type gtpases in the control of tip growth. *Plant Cell*, **9**, 1647–1659.

Manes, S., Ana Lacalle, R., Gomez-Mouton, C. and Martinez-A, C. (2003) From rafts to crafts: membrane asymmetry in moving cells. *Trends Immunol.* **24**, 319–325.

Martin, S.W. and Konopka, J.B. (2004) Lipid raft polarization contributes to hyphal growth in *Candida albicans*. *Eukaryot. Cell*, **3**, 675–684.

Mayor, S. and Rao, M. (2004) Rafts: scale-dependent, active lipid organization at the cell surface. *Traffic*, **5**, 231–240.

Messerli, M.A., Danuser, G. and Robinson, K.R. (1999) Pulsatile influxes of H^+, K^+ and Ca^{2+} lag growth pulses of Lilium longiflorum pollen tubes. *J. Cell Sci.* **112**, 1497–1509.

Mittler, R., Vanderauwera, S., Gollery, M. and Van Breusegem, F. (2004) Reactive oxygen gene network of plants. *Trends Plant Sci.* **9**, 490–498.

Mongrand, S., Morel, J., Laroche, J., Claverol, S., Carde, J.P., Hartmann, M.A., Bonneu, M., Simon-Plas, F., Lessire, R. and Bessoule, J.J. (2004) Lipid rafts in higher plant cells: purification and characterization of Triton X-100-insoluble microdomains from tobacco plasma membrane. *J. Biol. Chem.* **279**, 36277–36286.

Owen, D.M., Lanigan, P.M.P., Dunsby, C., Munro, I., Grant, D., Neil, M.A.A., French, P.M.W. and Magee, A.I. (2006) Fluorescence lifetime imaging provides enhanced contrast when imaging the phase-sensitive dye di-4-ANEPPDHQ in model membranes and live cells. *Biophys. J.* **90**, L80–L82.

Owen, D.M., Neil, M.A.A., French, P.M.W. and Magee, A.I. (2007) Optical techniques for imaging membrane lipid microdomains in living cells. *Semin. Cell Dev. Biol.* **18**, 591–598.

Papanikolaou, A., Papafotika, A., Murphy, C., Papamarcaki, T., Tsolas, O., Drab, M., Kurzchalia, T.V., Kasper, M. and Christoforidis, S. (2005) Cholesterol-dependent lipid assemblies regulate the activity of the ecto-nucleotidase CD39. *J. Biol. Chem.* **280**, 26406–26414.

Pei, Z.-M., Murata, Y., Benning, G., Thomine, S., Klusener, B., Allen, G.J., Grill, E. and Schroeder, J.I. (2000) Calcium channels activated by hydrogen peroxide mediate abscisic acid signalling in guard cells. *Nature*, **406**, 731–734.

Potocky, M., Jones, M.A., Bezvoda, R., Smirnoff, N. and Zarsky, V. (2007) Reactive oxygen species produced by NADPH oxidase are involved in pollen tube growth. *New Phytol.* **174**, 742–751.

del Pozo, M.A., Alderson, N.B., Kiosses, W.B., Chiang, H.-H., Anderson, R.G.W. and Schwartz, M.A. (2004) Integrins regulate Rac targeting by internalization of membrane domains. *Science*, **303**, 839–842.

Sagi, M. and Fluhr, R. (2001) Superoxide production by plant homologues of the gp91phox NADPH oxidase. Modulation of activity by calcium and by tobacco mosaic virus infection. *Plant Physiol.* **126**, 1281–1290.

Samaj, J., Baluska, F. and Menzel, D. (2004) New signalling molecules regulating root hair tip growth. *Trends Plant Sci.* **9**, 217–220.

Simons, K. and Toomre, D. (2000) Lipid rafts and signal transduction. *Nat. Rev. Mol. Cell Biol.* **1**, 31–39.

Sorek, N., Poraty, L., Sternberg, H., Bar, E., Lewinsohn, E. and Yalovsky, S. (2007) Activation status-coupled transient S acylation determines membrane partitioning of a plant Rho-related GTPase. *Mol. Cell. Biol.* **27**, 2144–2154.

Sun, Y., Qian, H., Xu, X.-d., Han, Y., Yen, L.-f. and Sun, D.-y. (2000) Integrin-like proteins in the pollen tube: detection, localization and function. *Plant Cell Physiol.* **41**, 1136–1142.

Takeda, T., Kawate, T. and Chang, F. (2004) Organization of a sterol-rich membrane domain by cdc15p during cytokinesis in fission yeast. *Nat. Cell Biol.* **6**, 1142–1144.

Takeda, S., Gapper, C., Kaya, H., Bell, E., Kuchitsu, K. and Dolan, L. (2008) Local positive feedback regulation determines cell shape in root hair cells. *Science*, **319**, 1241–1244.

Van Breusegem, F., Bailey-Serres, J. and Mittler, R. (2008) Unraveling the tapestry of networks involving reactive oxygen species in plants. *Plant Physiol.* **147**, 978–984.

Very, A.-A. and Davies, J.M. (2000) Hyperpolarization-activated calcium channels at the tip of Arabidopsis root hairs. *Proc. Natl Acad. Sci. USA*, 160250397.

Vilhardt, F. and van Deurs, B. (2004) The phagocyte NADPH oxidase depends on cholesterol-enriched membrane microdomains for assembly. *EMBO J.* **23**, 739–748.

Wachtler, V., Rajagopalan, S. and Balasubramanian, M.K. (2003) Sterol-rich plasma membrane domains in the fission yeast *Schizosaccharomyces pombe*. *J. Cell Sci.* **116**, 867–874.

Willemsen, V., Friml, J., Grebe, M., van den Toorn, A., Palme, K. and Scheres, B. (2003) Cell polarity and pin protein positioning in Arabidopsis require STEROL METHYLTRANSFERASE1 function. *Plant Cell*, **15**, 612–625.

Wong, H.L., Pinontoan, R., Hayashi, K. *et al.* (2007) Regulation of rice NADPH oxidase by binding of Rac GTPase to its N-terminal extension. *Plant Cell*, **19**, 4022–4034.

Xu, X., Bittman, R., Duportail, G., Heissler, D., Vilcheze, C. and London, E. (2001) Effect of the structure of natural sterols and sphingolipids on the formation of ordered sphingolipid/sterol domains (Rafts). *J. Biol. Chem.* **276**, 33540–33546.

Yang, B., Oo, T.N. and Rizzo, V. (2006) Lipid rafts mediate H_2O_2 prosurvival effects in cultured endothelial cells. *FASEB J.* **20**, 1501–1503.

